Erratum: {ldquo}Milky Way Red Dwarfs in the Borg Survey; Galactic Scale-Height and the Distribution of Dwarfs Stars in WFC3 Imaging`` (2014, ApJ, 788, 77)

Holwerda, B.W.; Trenti, M.; Clarkson, W.; Sahu, K.; Bradley, L.; Stiavelli, M.; ... ; Vlugt, D.

The Astrophysical Journal, 825:82 (5pp), 2016 July 1 doi:10.3847/0004-637X/825/1/82

ERRATUM: "MILKY WAY RED DWARFS IN THE BORG SURVEY; GALACTIC SCALE-HEIGHT AND THE DISTRIBUTION OF DWARFS STARS IN WFC3 IMAGING" (2014, ApJ, 788, 77)

B. W. Holwerda[1,2,7,8], M. Trenti[3], W. Clarkson[4], K. Sahu[5], L. Bradley[5], M. Stiavelli[5], N. Pirzkal[5], G. De Marchi[2], M. Andersen[6], R. Bouwens[1], R. Ryan[5], I. van Vledder[1], and D. van der Vlugt[1]
[1] Leiden Observatory, Leiden University, P.O. Box 9513, 2300 RA Leiden, The Netherlands; holwerda@strw.leidenuniv.nl
[2] European Space Agency, ESA-ESTEC, Keplerlaan 1, 2200 AG Noordwijk, The Netherlands
[3] School of Physics, University of Melbourne, VIC 3010, Australia
[4] Department of Natural Sciences College of Arts, Sciences and Letters, University of Michigan-Dearborn 4901 Evergreen Road, Dearborn, MI:48128, USA
[5] Space Telescope Science Institute, Baltimore, MD 21218, USA
[6] UJF-Grenoble 1/CNRS-INSU, Institut de Planétologie et d'Astrophysique de Grenoble (IPAG) UMR 5274, Grenoble, F-38041, France
Received 2015 October 20; revised 2016 February 3; accepted 2016 February 3; published 2016 July 5

ABSTRACT

In the catalog of M-dwarfs presented in Holwerda et al. (2014, H14 hereafter), there is an issue with the conversion from celestial coordinates to Galactic ones, done with PYEPHEM a wrapper around a trusted and vetted library *ephermis*. Here we present the corrected coordinates (using AstroPy) and distances based on AB magnitudes. We have amended the tables and figures accordingly. The relation between vertical scale-height (z_0) and M- dwarf subtype found in H14 is no longer present. We find a scale-height of 600 pc for all types, in part due to the presence of a second Galactic structural component.

1. MAPPING THE M-DWARF DISTRIBUTION

We re-computed the Galactic coordinates for the BoRG fields using the AstroPy package (Astropy Collaboration et al. 2013) and the number of M-dwarfs in each, shown in the new Figure 22. The new values for all identified M-dwarfs are listed in Table 14. To estimate the distances to each M-dwarf, we compute the distance modulus from the inferred sub-type (and hence absolute magnitude) and the apparent magnitude in J_{F125W} from Hawley et al. (2002), converted from Vega magnitudes to AB. We compute the Galactic radius and height above the plane for all M-dwarfs, based on their Galactic longitude, latitude and the inferred photometric distances, assuming the position of the Sun 27 pc. above the plane and 8.5 kpc from the Galactic center.

The net difference with Holwerda et al. (2014, H14 hereafter) is that the vertical distribution observed for these M-dwarfs is much closer to the exponential drop-off one would expect for fields out of the plane of the Galaxy.

Figure 24 shows the vertical distribution of M-dwarfs color-coded by their Galactocentric radius. There is a clear disk component with all the M-dwarfs are ~6–10 kpc from the center of the Milky Way and another component which shows a gradient with radius and is well above the plane of the disk. We now know this component to be the Halo part of the vertical distribution (van Vledder et al. 2016) but it is sometimes treated as the thick disk by other authors (e.g., Ryan & Reid 2016). This second component is much clearer in the corrected Galactic positions compared to H14. The majority of stars close to the plane of the disk are ~8 kpc from the center of the Galaxy. This is because the majority of BoRG fields are pointing out of the disk at an angle away from the Galactic Center (to avoid confusion with Galactic Objects) and thus probe the vertical extent of the disk close to the position of the Sun.

We assume there is no need to correct the densities in this part of the disk for the exponential decline with radius. Figure 24 does show a radial dependence of the outer parts of the vertical distribution on the radius. Our assumption is that the scale-height does not change significantly with radius, which is observed in external galaxies seen edge-on (Comerón et al. 2011a, 2011a, 2011c, Streich et al. 2016 in preparation).

We assume that the Galactic disk has the following parametric shape:

$$\rho(R, z) = \rho_0 \exp(-R/h) sech^2\left(\frac{z}{2 \times z_0}\right), \quad (1)$$

where $\rho(R, z)$ is the dwarf number density in a point in the disk, ρ_0 is the central number density, R is Galactocentric radius, h is the scale-length, z is height above the plane, and z_0 is the exponential scale-height of the disk. Figure 25 shows how the later-type M-dwarfs (M4-8) in the BoRG fields are concentrated in the thin disk and the earlier types (M0-3) probe both thin disk and the other component. We fit the $sech^2$ distribution to each photometric subtype, as well as early-, late- and all-types of M-dwarfs, summarized in the new Table 10 and the new Figures 26 and 27.

Figures 26 and 27 are significantly different from the versions in H14 in two ways: the relation between vertical scale-height (z_0) and M- dwarf subtype found in H14 is no longer present in Figure 27. Second, the densities inferred are much closer to the local (<20 pc of the Sun) Reid et al. (2004) and Cruz et al. (2007) values (Figure 26). We note there is an offset of ~0.1 dex between our central density and the one implied by Reid et al. The likely culprit is the additional numbers of M-dwarfs in the secondary

[7] twitter:benneholwerda.
[8] Research Fellow.

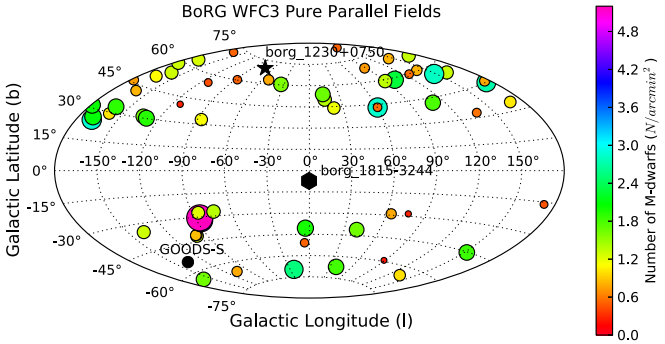

Figure 22. The Aitoff projection of the distribution of BoRG fields with the surface density of M-dwarfs of all types indicated. One field, borg_1230+0750 (star) stands out with 22 M-dwarfs (~5 stars arcmin^{-2}). We discard borg_1815-3244 (black circle) for its low latitudes and line-of-sight through the plane of the disk and close of the center of the bulge.

Table 10
The Vertical Profile Fits to The Full Sample of Identified M-dwarfs

M-type (∘)	ρ_0 ($\#/pc^3$)	z_0 (kpc)
0	0.02	0.67 ± 0.73
1	0.19	0.84 ± 0.89
2	0.06	0.80 ± 1.31
3	0.60	0.61 ± 12.36
4	0.14	1.04 ± 0.67
5	0.77	0.67 ± 0.74
6	2.49	1.03 ± 5.42
7	…	…
8	181.04	−0.01 ± 0.02

Note. Values are Scaled so to be Compatible with Exponential Fits to The Galactic Profiles ($\rho_0/4$ and $z_0/2$).

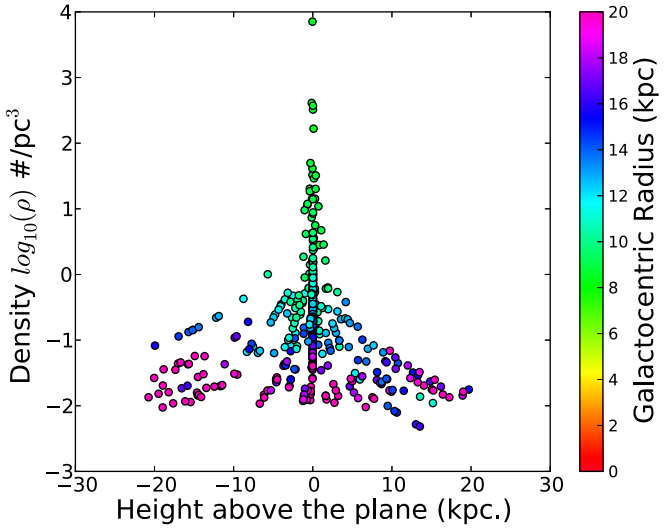

Figure 24. The volume density of M-dwarfs as a function as height above the plane of the Milky Way disk. The volume densities were normalized with a scale-length of 2.6 kpc and a depth of 1pc at each star's position. Points are color-coded by the inferred Galactic radius. The majority of M-dwarfs are found close to the plane of the disk.

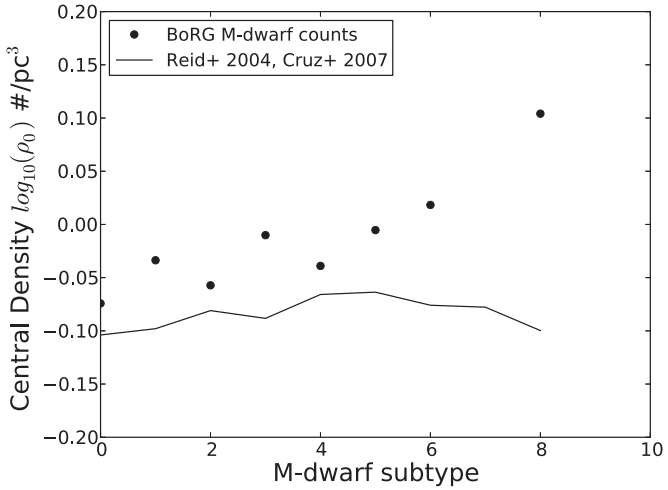

Figure 26. The in-plane central density—the number of M-dwarfs belonging to the disk at the center of the Milky Way–for the best fit to the vertical distribution of M-dwarfs as a function of the M-dwarf subtype. The black circles are the values from Reid et al. (2008) for the immediate Solar neighborhood (<20 pc), renormalized to the center of the Milky Way.

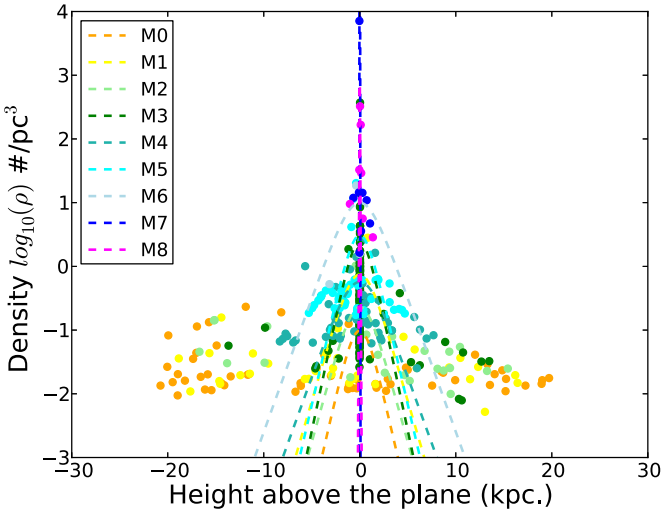

Figure 25. The volume density of M-dwarfs as a function as height above the plane of the Milky Way disk. Points and fits are color-coded by the M-dwarf sub-type.

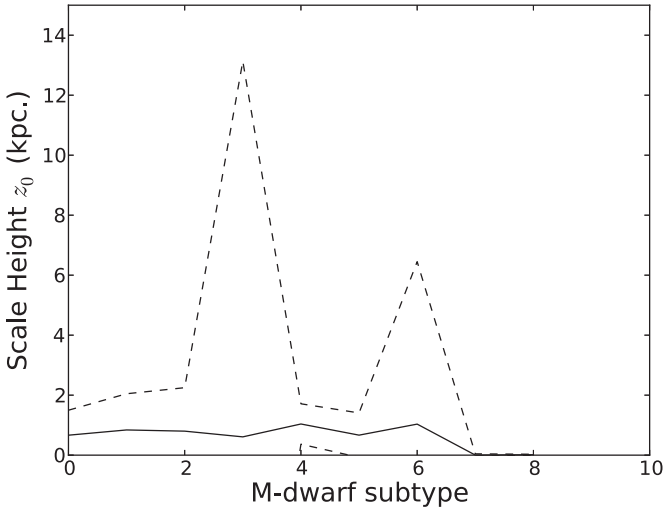

Figure 27. The scale-height ($z_0/2$) of the best vertical fit as a function of the M-dwarf subtype. Dashed lines are the uncertainty in the fit. A constant value of 600 pc would be consistent with most of these fits. This is ~2× greater than expected from previous work.

Table 14
The 274 M-dwarfs Identified in BoRG

ID	R.A.	Decl.	l	b	m_{F098M}	m_{F125W}	m_{F125W}	m_{F606W}	Mtype	modulus	dist	Height	Radius	Volume	Area
borg_0110-0224.551.0	17.501759	−2.418265	133.918256	−64.893095	23.82 ± 0.04	23.46 ± 0.02	23.28 ± 0.03	25.17 ± 0.09	2.04 ± 0.32	16.48	19.74	14.25	16.88 ± 1.85	228.43	10.88
borg_0110-0224.719.0	17.503586	−2.415663	133.921454	−64.890220	24.33 ± 0.05	23.97 ± 0.03	23.87 ± 0.04	25.83 ± 0.14	2.56 ± 0.50	16.73	22.16	15.99	17.90 ± 2.73	287.73	10.88
borg_0110-0224.820.0	17.528020	−2.411389	133.976421	−64.881854	19.68 ± 0.00	19.51 ± 0.00	19.45 ± 0.00	22.77 ± 0.01	7.30 ± 0.04	8.59	0.52	0.40	8.72 ± 0.01	0.16	10.88
borg_0110-0224.1016.0	17.553100	−2.408888	134.033565	−64.875102	24.54 ± 0.09	23.90 ± 0.04	23.72 ± 0.05	25.39 ± 0.13	1.30 ± 0.46	17.18	27.26	19.63	20.08 ± 3.83	435.66	10.88
borg_0110-0224.1414.0	17.559120	−2.400783	134.044244	−64.866085	24.08 ± 0.06	23.71 ± 0.06	23.44 ± 0.04	24.40 ± 0.05	−1.43 ± 0.27	17.26	28.31	20.37	20.52 ± 687.31	469.66	10.88

Table 15
The 1 T-Dwarfs Identified in BoRG

ID	R.A.	Decl.	l	b	m_{F098M}	m_{F125W}	m_{F125W}	m_{F606W}
borg_0540-6409.1929.0	84.862502	−64.152446	84.862502	−64.152446	22.9 ± 0.0	21.9 ± 0.0	22.2 ± 0.0	21.5 ± 0.0

Table 16
The 30 L-Dwarfs Identified in BoRG

ID	R.A.	Decl.	l	b	m_{F098M}	m_{F125W}	m_{F125W}	m_{F606W}
borg_0110-0224.1010.0	17.537240	−2.409470	17.537240	−2.409470	24.7 ± 0.1	23.7 ± 0.0	23.5 ± 0.0	25.3 ± 0.1
borg_0439-5317.882.0	69.836642	−53.263207	69.836642	−53.263207	24.0 ± 0.0	22.7 ± 0.0	22.2 ± 0.0	24.8 ± 0.9
borg_0540-6409.2993.0	84.876906	−64.132531	84.876906	−64.132531	25.0 ± 0.1	23.8 ± 0.0	23.4 ± 0.0	26.8 ± 0.6
borg_0751+2917.567.0	117.684321	29.285619	117.684321	29.285619	19.5 ± 0.0	17.8 ± 0.0	17.6 ± 0.0	19.6 ± 0.0
borg_0808+3946.457.0	122.094091	39.759095	122.094091	39.759095	25.0 ± 0.1	23.9 ± 0.0	23.5 ± 0.0	26.9 ± 0.6
borg_0819+4911.264.0	124.831743	49.175806	124.831743	49.175806	23.9 ± 0.0	22.8 ± 0.0	22.4 ± 0.0	27.9 ± 1.6
borg_0906+0255.462.0	136.409407	2.923645	136.409407	2.923645	24.4 ± 0.0	23.3 ± 0.0	22.8 ± 0.0	27.6 ± 0.8
borg_0909+0002.748.0	137.292821	−0.012257	137.292821	−0.012257	24.5 ± 0.1	23.2 ± 0.0	22.8 ± 0.3	26.6 ± 0.4
borg_0914+2822.673.0	138.558022	28.364206	138.558022	28.364206	24.8 ± 0.1	23.5 ± 0.0	23.1 ± 0.0	26.3 ± 0.3
borg_0926+4426.581.0	141.355847	44.425445	141.355847	44.425445	24.3 ± 0.0	23.1 ± 0.0	22.6 ± 0.0	25.2 ± 0.9
borg_1103-2330.623.0	165.819910	−23.506010	165.819910	−23.506010	23.9 ± 0.1	22.9 ± 0.0	22.5 ± 0.0	25.7 ± 0.2
borg_1111+5545.1125.0	167.747157	55.771759	167.747157	55.771759	23.6 ± 0.0	22.5 ± 0.0	22.1 ± 0.0	26.6 ± 0.3
borg_1153+0056.247.0	178.200215	0.922794	178.200215	0.922794	23.9 ± 0.0	22.9 ± 0.0	22.4 ± 0.0	26.2 ± 0.3
borg_1230+0750.2419.0	187.471709	7.820117	187.471709	7.820117	23.9 ± 0.1	22.8 ± 0.0	22.3 ± 0.0	26.2 ± 0.3
borg_1301+0000.1067.0	195.326828	0.013297	195.326828	0.013297	23.5 ± 0.1	22.2 ± 0.0	21.8 ± 0.0	24.3 ± 0.9
borg_1337+0028.1117.0	204.205278	−0.445870	204.205278	−0.445870	24.3 ± 0.2	23.1 ± 0.0	22.7 ± 0.0	25.3 ± 0.9
borg_1524+0954.24.0	231.044740	9.885957	231.044740	9.885957	24.9 ± 0.1	23.0 ± 0.1	22.8 ± 0.1	25.3 ± 1.0
borg_1632+3733.65.0	248.069017	37.540353	248.069017	37.540353	24.5 ± 0.0	23.3 ± 0.0	22.9 ± 0.0	28.5 ± 2.1
borg_1632+3733.349.0	248.080963	37.550065	248.080963	37.550065	23.5 ± 0.0	22.4 ± 0.0	22.0 ± 0.1	27.1 ± 1.4
borg_1632+3733.1325.0	248.076265	37.572819	248.076265	37.572819	24.3 ± 0.0	23.0 ± 0.1	22.5 ± 0.0	26.7 ± 0.5
borg_2132+1004.284.0	323.058751	10.068991	323.058751	10.068991	16.8 ± 0.0	15.0 ± 0.0	14.7 ± 0.0	17.2 ± 0.9
borg_2132+1004.332.0	323.060235	10.059801	323.060235	10.059801	21.2 ± 0.0	19.9 ± 0.0	19.7 ± 0.0	22.2 ± 0.9
borg_2155-4411.227.0	328.831076	−44.185153	328.831076	−44.185153	23.5 ± 0.0	22.5 ± 0.0	22.2 ± 0.0	24.8 ± 0.9
borg_2155-4411.974.0	328.809893	−44.164189	328.809893	−44.164189	24.3 ± 0.0	23.0 ± 0.0	22.5 ± 0.0	25.1 ± 0.9
borg_2351-4332.1314.0	357.668728	−43.514053	357.668728	−43.514053	25.2 ± 0.1	23.9 ± 0.0	23.5 ± 0.0	26.0 ± 0.9
borg_0456-2203.920.0	73.945566	−22.049396	73.945566	−22.049396	24.6 ± 0.1	23.4 ± 0.0	23.2 ± 0.0	24.4 ± 0.0
borg_1059+0519.644.0	164.717943	5.301323	164.717943	5.301323	24.4 ± 0.0	23.1 ± 0.0	22.6 ± 0.0	26.5 ± 0.3
borg_1118-1858.1915.0	169.392755	−18.972497	169.392755	−18.972497	24.8 ± 0.0	23.8 ± 0.0	23.3 ± 0.0	26.1 ± 0.1
borg_1459+7146.1298.0	224.751450	71.780685	224.751450	71.780685	24.8 ± 0.2	23.5 ± 0.0	23.1 ± 0.0	25.7 ± 0.1
borg_2132-1202.6461.0	322.941469	−12.021619	322.941469	−12.021619	24.6 ± 0.1	23.4 ± 0.0	23.0 ± 0.0	26.5 ± 0.4

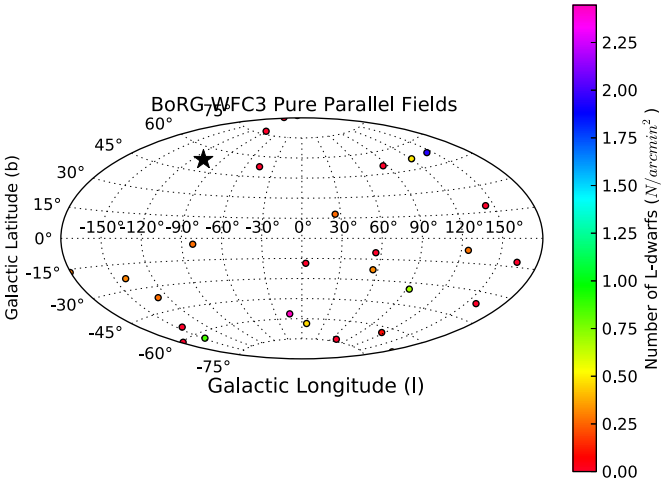

Figure 28. The distribution of BoRG fields with the number of L-dwarfs indicated. Other symbols identical to Figure 22.

component well above the plane of the disk, i.e., we are including the density of Halo stars in our disk fit. A 0.1 dex offset suggest of order 10% of the stars in are, in fact, Halo stars (see also van Vledder et al. 2016).

The values in Figure 27 and Table 10 are still too high to be consistent with previous work on the vertical scale of stars in the thin disk. The vertical $sech^2$ profile does not describe the density distribution well above ~500 pc and this new distributions highlights the need to include another component well above and in addition to the disk.

For completeness, we include Figure 28 which shows the surface density of L-dwarfs selected by our morphology and color criteria.

2. CONCLUSIONS

The majority of conclusions for Holwerda et al. (2014) remain the same, only the last two change:

1. The secondary component visible in the vertical distribution of M-dwarfs is likely the Halo and not the thick disk of the Milky Way (Figures 24 and 25).
2. A naive, single-component fit of the vertical distribution of M-dwarfs shows no dependence on M-dwarf subtype and a scale-height for all M-dwarf subtypes that is still too high to be consistent with previous measures of the scale-height: $z_0 \sim 600$ pc, (Figure 27), a result of the second structural component.

The authors would like to thank the referee, K. Cruz for her help with the erratum. This research made use of Astropy, a community-developed core Python package for Astronomy (Astropy Collaboration et al. 2013). This research made use of matplotlib, a Python library for publication quality graphics (Hunter 2007). PyRAF is a product of the Space Telescope Science Institute, which is operated by AURA for NASA. This research made use of SciPy (Jones et al. 2001).

REFERENCES

Astropy Collaboration, Robitaille, T. P., Tollerud, E. J., et al. 2013, A&A, 558, A33
Comerón, S., Elmegreen, B. G., Knapen, J. H., et al. 2011b, ApJ, 738, L17
Comerón, S., Elmegreen, B. G., Knapen, J. H., et al. 2011c, ApJ, 741, 28
Comerón, S., Knapen, J. H., Sheth, K., et al. 2011c, ApJ, 729, 18
Cruz, K. L., Reid, I. N., Kirkpatrick, J. D., et al. 2007, AJ, 133, 439
Hawley, S. L., Covey, K. R., Knapp, G. R., et al. 2002, AJ, 123, 3409
Holwerda, B. W., Trenti, M., Clarkson, W., et al. 2014, ApJ, 788, 77
Hunter, J. D. 2007, Computing In Science & Engineering, 9, 90
Jones, E., Oliphant, T., Peterson, P., et al. 2001, SciPy: Open source scientific tools for Python
Reid, I. N., Cruz, K. L., Allen, P., et al. 2004, AJ, 128, 463
Reid, I. N., Cruz, K. L., Kirkpatrick, J. D., et al. 2008, AJ, 136, 1290
Ryan, R. E., Jr., & Reid, I. N. 2016, AJ, 151, 92
van Vledder, Is., van der Vlugt, D., Holwerda, B. W., Kenworthy, M. A., Bouwens, R. J., & Trenti, M. 2016, MNRAS, 458, 425